Immortalized mouse embryo fibroblasts are resistant to miR-290-induced senescence regardless of p53 status

Milena Rizzo, Monica Evangelista, Laura Mariani, Marcella Simili, Giuseppe Rainaldi and Letizia Pitto

Physiol. Genomics 43:1153-1159, 2011. First published 16 August 2011;
doi:10.1152/physiolgenomics.00064.2011

Physiological Genomics publishes results of a wide variety of studies from human and from informative model systems with techniques linking genes and pathways to physiology, from prokaryotes to eukaryotes. It is published quarterly in January, April, July, and October by the American Physiological Society, 9650 Rockville Pike, Bethesda MD 20814-3991. ISSN: 1094-8341, ESSN: 1531-2267. Visit our website at http://www.the-aps.org/.

Physiol Genomics 43: 1153–1159, 2011.
First published August 16, 2011; doi:10.1152/physiolgenomics.00064.2011.

Immortalized mouse embryo fibroblasts are resistant to miR-290-induced senescence regardless of p53 status

Milena Rizzo,[1] Monica Evangelista,[1] Laura Mariani,[1] Marcella Simili,[1] Giuseppe Rainaldi,[1,2] and Letizia Pitto[1]

[1]*Laboratory of Gene and Molecular Therapy, Institute of Clinical Physiology, Consiglio Nazionale delle Ricerche, Pisa; and* [2]*Istituto Toscano Tumori, Firenze, Italy*

Submitted 29 April 2011; accepted in final form 10 August 2011

Rizzo M, Evangelista M, Mariani L, Simili M, Rainaldi G, Pitto L. Immortalized mouse embryo fibroblasts are resistant to miR-290-induced senescence regardless of p53 status. *Physiol Genomics* 43: 1153–1159, 2011. First published August 16, 2011; doi:10.1152/physiolgenomics.00064.2011.—The prosenescence role of miR-290 and nocodazole has been documented in primary mouse embryo fibroblasts (MEF), while it is not clear whether immortal murine fibroblasts are still responsive to these senescence inducing stimuli. To establish this point, immortal murine fibroblasts with functional (NIH3T3) or nonfunctional p53 (I-MEF) and low levels of miR-290 were tested for their capability to undergo senescence after exposure to either nocodazole or miR-290. Our results clearly indicate that nocodazole induces senescence only in NIH3T3 cells with a functional p53 but not in I-MEF lacking a functional p53. miR-290 overexpression is unable to address any of the tested immortalized clones toward senescence, regardless of the p53 status, suggesting that the prosenescence role of miR-290 is specific for primary but not for immortal murine fibroblasts. Moreover our findings suggest that the mere downregulation of a potential tumor suppressor miRNA in a given cell type does not necessarily imply that it behaves as a tumor suppressor.

microRNA-290; nocodazole

THE LIFE SPAN of mouse embryo fibroblasts (MEF) under the 6T3 propagation regimen is very short: after 4–5 passages it is exhausted and an appreciable fraction of cells become senescent acquiring a flat morphology and a positivity to pH 6.0 senescence-associated β-galactosidase (SA-β-gal)$^+$ cells staining (2, 8). In line with the progressive increase of SA-β-gal$^+$ cells is the enhanced expression of p19ARF and p16, both encoded by the *INK4a/ARF* locus (14). p19ARF activates the tumor suppressor p53 by inhibiting MDM2 thus preventing p53 ubiquitination (16), while p16 inhibits cyclin-dependent protein kinases, thereby activating retinoblastoma, which blocks E2F1 and the cell cycle (13). p21, another cyclin-dependent kinase inhibitor under p53 control (5), also increases during senescence (9). We have shown that MEF population in culture is characterized not only by the increase of p19ARF, p16, and p21 but also by a progressive accumulation of cells with 4C DNA content (9). These cells are probably G1 tetraploid cells, which, in the presence of wild-type p53, do not progress into the cell cycle and undergo senescence (9). It is known that a prolonged tetraploid G1 arrest addresses p53-positive cells toward senescence (15), in accordance with the concept that senescence is a tumor suppressor mechanism by which cells potentially prone to transformation are eliminated (2). The analysis of microRNA (miRNA or miR) expression levels in senescent MEF revealed that the entire miR-290–295 cluster increases during senescence, reaching the highest expression when the shift from 2C to 4C is fully accomplished (9). The prosenescence role of miR-290 was verified by overexpressing this miRNA in early passage MEF (P-MEF), where it induced premature senescence. In accordance with these findings we observed increased miR-290 expression after prolonged treatment of MEF with nocodazole (NCZ), which induced both tetraploid G1 and SA-β-gal$^+$ cells (9).

It is known that MEF, during the immortalization process, escape senescence by functionally eliminating some of the above-mentioned tumor suppressor genes. In MEF, extensively used as a model system to study senescence and immortalization, the functional silencing of either the *INK4a/ARF* locus (10) or p53 (3) appears to be necessary steps to bypass senescence.

As the prosenescence role of miR-290 and NCZ was demonstrated in primary MEF, with functional cell cycle check points (*INK4a/ARF* locus and p53) (9), it was interesting to ask whether immortalized MEF are still responsive to these stimuli. To verify this point, clones from immortalized MEF (immortalized clones, I-clones) as well as NIH3T3 were tested for their capability to undergo senescence after either miR-290 transfection or NCZ treatment.

MATERIALS AND METHODS

Reagents. We used the following: mature miR-290 and double-stranded oligonucleotide negative control (miR-NC) (GenePharma, Shanghai, China); Gene Silencer (Gene Therapy Systems, San Diego, CA); oligo-FITC (IFC, Pisa, Italy); miRNeasy mini kit, QuantiTect Reverse Transcription Kit, miScript Reverse Transcription Kit, miScript SYBR Green PCR Kit (QIAGEN, Milano, Italy); Dulbecco's modified eagle medium-high glucose (DMEM-HG), Optimem, fetal bovine serum (FBS) (Invitrogen, Carlsbad, CA); LightCycler 480 Probes Master, Universal Probe Library LNA Probes; LightCycler 480 SYBR Green I Master (Roche Diagnostic, Mannheim, Germany); X-Gal (5-bromo-4-chloro-3-indolylb-D-galactoside); propidium iodide, crystal violet, NCZ; anti-α-tubulin (Sigma-Aldrich, St. Louis, MO); anti-p16, anti-p21 (Santa Cruz Biotechnology); ECL, Hybond-C extra membranes (Amersham); anti-p19ARF (ab Cam); Nutlin-3 (a kind gift by Dr. G. Del Sal).

Cells and culture conditions. MEF were isolated from 13.5-day mouse embryos, expanded, and then replated every 3 days (9). Colonies isolated from postsenescence MEF were expanded to obtain clonal populations (named I-clones) to be used for the analyses. MEF and derived clones were grown in DMEM-HG-10% FBS. NIH3T3 were grown in Dulbecco's modified Eagle's medium-low glucose

Address for reprint requests and other correspondence: G. Rainaldi, Laboratory of Gene and Molecular Therapy, Institute of Clinical Physiology, Area della Ricerca CNR, Via Moruzzi 56124 Pisa, Italy (e-mail: g.rainaldi@ifc.cnr.it).

(DMEM-LG)-10% FBS. All cell types were incubated at 37°C in a humidified atmosphere containing 6% CO_2.

Cell proliferation. Cell proliferation was measured as number of cell doublings per passage (CD) = $\ln(N_f/N_i)/\ln 2$, where N_f is the final number of collected cells (*day 3*) and N_i the initial number of seeded cells (*day 0*).

Quantification of miRNAs and genes with real-time PCR. Total RNA was extracted from 1×10^6 cells using the miRNeasy mini kit (Qiagen) following the manufacturer's recommendations. To quantify p19ARF, p16, and p21 transcripts, 1 μg of total RNA was reverse transcribed using QuantiTect Reverse Transcription Kit (Qiagen). Real-time PCR (qRT-PCR) was carried out with LightCycler 480 (Roche) using LightCycler 480 SYBER Green I Master (Roche). Mature miR-290, miR-291–3p, miR-292–3p, and miR-295 were quantified using the miScript System: 1 μg of total RNA was retrotranscribed with miScript Reverse Transcription Kit (Qiagen) and qRT-PCR was carried out using miScript SYBR Green PCR Kit (Qiagen). All reactions were performed in triplicate. Relative quantification of genes and miRNAs expression was calculated with the fit point method. Transcript values were normalized with those obtained from the amplification of the internal controls (GAPDH for transcripts and U6 for miRNAs). The expression values of the miR-290–295 cluster were converted into a heat map using JcolorGrid (6). The following oligonucleotides were used: p19ARF, forward (F) (5′-CATGGGTCGCAGGTTCTTG-3′) and reverse (R) (5′-GCTCGCTGTCCTGGGTCTC-3′); p16, F (5′-CGACGGGCATAGCTTCAG-3′) and R (5′-GCTCTGCTCTTGGGATTGG-3′); p21, F (5′-TCCACAGCGATATCCAGACA-3′) and R (5′-GGACATCACCAGGATTGGAC-3′); p53, F (5′-ATGCCCATGCTACAGAGGAG-3′) and R (5′-AGACTGGCCCTTCTTGGTCT-3′); GAPDH, F (5′-GCCTTCCGTGTTCCTACCC-3′), R (5′-TGCCTGCTTCACCACCTTC-3′); miR-290, F (5′-ACTCAAACTATGGGGGCACTTT-3′); miR-291–3p, F (5′-AAAGTGCTTCCACTTTGTGTGC-3′); miR-291–3p, F (5′-AAAGTGCTTCCACTTTGTG TGC-3′); miR-292–3p, F (5′-AAAGTGCCGCCAGGTTTTGAGTGT-3′); miR-295, F (5′-AAAGTGCTactactttgagtct-3′); U6, F (5′-CGCAAGGATGACACGCAAATTC-3′).

Western blot analysis. Equivalent amounts of proteins were resolved on 12% SDS-PAGE gels and transferred to Hybond-C extra membranes by electro-blotting. The resulting blots were blocked with 5% nonfat dry milk solution. Anti-α-tubulin (1:1,000), anti-p19ARF (1:2,000), anti-p16 (1:200) and anti-p21 (1:1,000) were used. Incubation was performed overnight at 4°C, and bands were revealed after incubation with the recommended secondary antibody coupled to peroxidase using ECL. Scanned images were quantified using Scion Image software and normalized to α-tubulin.

SA β-gal activity. In brief, 2×10^4 cells were seeded in 30 mm diameter dishes, and 24 h later dishes were washed once with PBS and fixed for 3–5 min at room temperature in PBS containing 2% formaldehyde-0.2% glutaraldehyde. Cells were then washed three times with PBS and incubated at 37°C with fresh SA β-gal$^+$ staining solution containing 1 mg/ml 5-bromo-4-chloro-3-indolyl P3-D-galactoside (X-Gal) (stock = 20 mg/ml in DMSO), 5 mM potassium ferrocyanide, 5 mM potassium ferricyanide, 2 mM $MgCl_2$ in PBS pH 6.0. After 24 h cells were washed in PBS and stained with 20 μg/ml Hoechst 33342 for 10 min. Dishes were scored with a Leica ILDM inverted microscope to count SA-β-gal$^+$ cells and Hoechst-positive nuclei. The ratio SA-β-gal$^+$ cells/Hoechst-positive nuclei of 10 consecutive fields (~750 nuclei) was used to determine the frequency of the event.

Cell cycle. Samples of 5×10^5 of cells under test were fixed with 95% ethanol, stained with 50 μg/ml propidium iodide, and incubated overnight at 4°C, and cell cycle was analyzed on a FACScalibur cytofluorimeter.

Colony forming ability. Cells under test were seeded at a density of 1×10^3 per 100 mm dish, and 10 days later dishes were stained with 2% crystal violet. The colony-forming ability was calculated by the ratio (number of colonies formed/number of seeded cells).

miR-290 transfection. Cells under test were seeded at cell density of 1.0×10^5 per 30 mm diameter dish. After 24 h cells were transfected with either miR-290 or a double-stranded oligonucleotide, named miR-NC. Briefly, 15 μl Optimem and 25 μl transfection buffer plus 80 nM miRNA were mixed with a solution of Gene Silencer (5 μl) plus Optimem (25 μl). After 15 min incubation, Optimem was added up to 800 μl. Then, the transfection mixture was added to 30 mm diameter dishes seeded with 1.5×10^5 cells 24 h earlier. After 6 h the medium was replaced with complete DMEM. Cells were collected at 48 h posttransfection and used for the detection of SA-β-gal$^+$ cells.

NCZ treatment. I-clones and NIH3T3 fibroblasts were seeded at cell density of 5×10^5 per 100 mm diameter dish. After 24 h culture medium was replaced with medium containing NCZ (50 ng/ml), and 16 h later cells were collected and used to detect cell cycle, SA-β-gal$^+$ cells and miR-290–295 cluster expression.

Nutlin-3 treatment. P-MEF, immortalized MEF (I-MEF), I-5 clone, and NIH3T3 fibroblasts were seeded at cell density of 3×10^5 per 100 mm diameter dish. After overnight incubation, culture medium was replaced with medium containing 10 μM nutlin-3, and 24 h later cells were collected and used to detect p21 expression.

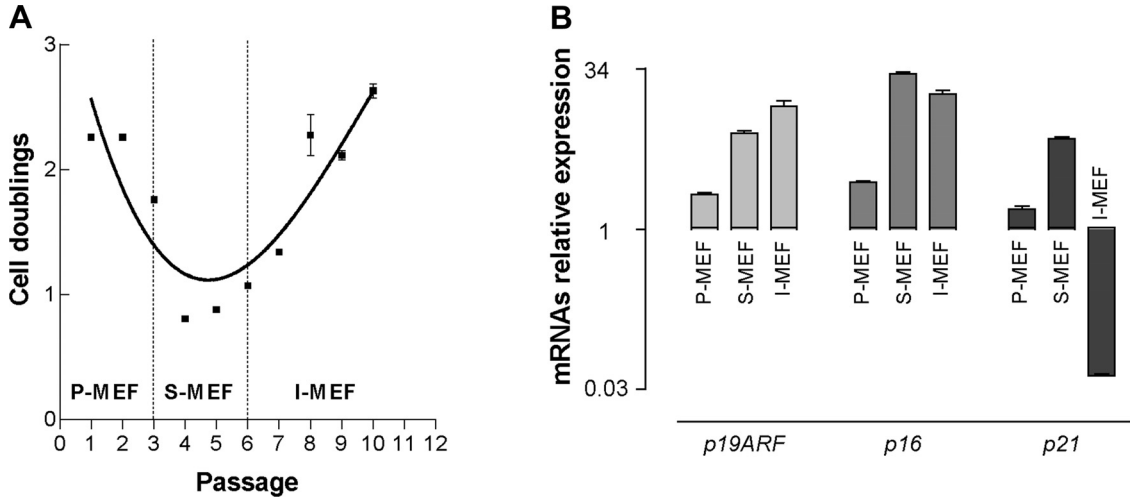

Fig. 1. Characterization of mouse embryo fibroblasts (MEF) under 6T3 propagation regimen. *A*: proliferation curve of MEF expressed as cell doublings per passage. Primary MEF (P-MEF), senescent MEF (S-MEF), and immortalized MEF (I-MEF) were distinguished on the basis of cell doublings. *B*: expression of *p19ARF*, *p16,* and *p21* mRNAs in P-MEF, S-MEF, and I-MEF normalized to that of MEF at *passage 0*; each bar represents the mean ± SD of 3 biological replicates.

Statistical analysis. Data were analyzed using GraphPad Prism (GraphPad Software, San Diego, CA). Comparisons were evaluated by unpaired *t*-test. Values of $P < 0.05$ (*), $P < 0.01$ (**), and $P < 0.001$ (***) were considered statistically significant.

RESULTS AND DISCUSSION

It is known that MEF escape senescence and acquire a proliferative phenotype after continuous propagation in culture

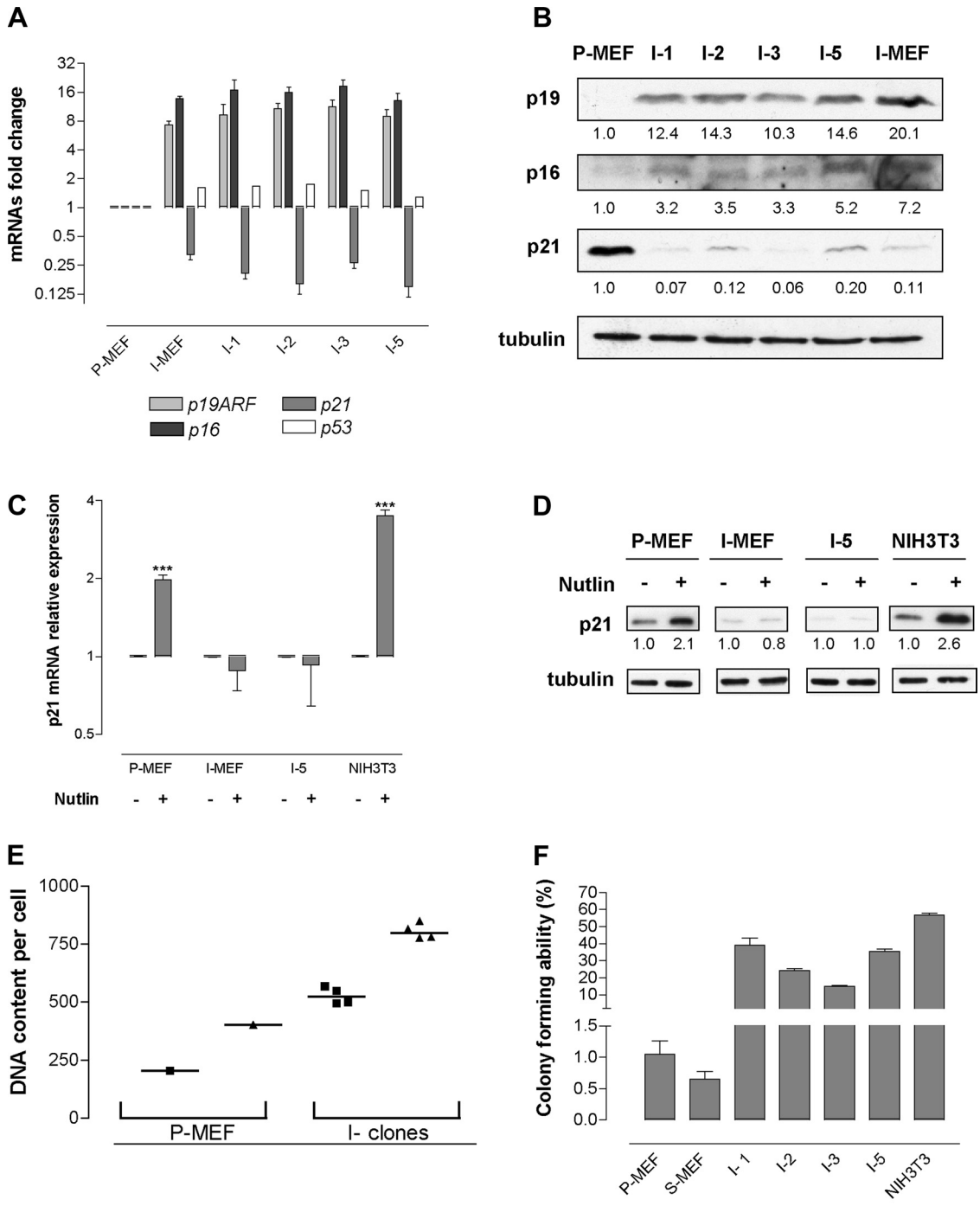

Fig. 2. Molecular and cellular characterization of I-clones. *A*: expression level of *p19ARF*, *p16*, *p53,* and *p21* in I-clones (I-1, 2, 3, 5) normalized to that of P-MEF; each bar represents the mean ± SD of 3 biological replicates. *B*: Western blot of p19ARF, p16, and p21 in I-clones and I-MEF normalized to that of P-MEF; the value reported under each lane represents the average of 2 experiments. *C*: expression of p21 in P-MEF, I-MEF, I-5, and NIH3T3 after 24 h treatment with 10 μM nutlin-3; each bar represents the mean ± SD of 3 biological replicates. *D*: Western blot of p21 in P-MEF, I-MEF, I-5, and NIH3T3 after 24 h treatment with 10 μM nutlin-3; the value reported under each lane represents the average of 2 experiments. *E*: DNA content profiles determined after propidium iodide (PI) staining of P-MEF and I-clones. *F*: colony forming ability of P-MEF, S-MEF, and I-clones; each bar represents the mean ± SD of 3 biological replicates.

(3). In our case, the onset of proliferating MEF occurred at *passage 6* and thereafter I-MEF fully replaced senescent MEF (S-MEF) (Fig. 1*A*). As the functional loss of either the *INK4a/ARF* locus and/or p53 (3, 18) is often associated with the escape from senescence the levels of *p16* and *p19ARF* as well as that of *p21* (under p53 control) transcripts were determined in P-MEF, S-MEF, and I-MEF. As expected the level of *p19ARF*, *p16,* and *p21* mRNAs was greater in S-MEF than in P-MEF. An interesting change is observed in I-MEF where the expression of p21 dramatically diminished, while p19ARF and p16 were still highly transcribed (Fig. 1*B*). Collectively, these results suggest that I-MEF have a functional loss of p53, while the *INK4a/ARF* locus remains expressed. Analogously all the clones isolated from I-MEF population (named I-1, 2, 3, 5), showed upregulation of both *p19ARF* and *p16* and downregulation of *p21,* while *p53* mRNA level remained constant (Fig. 2*A*). The protein levels of p19ARF, p16, and p21 were in accordance with the transcript levels (Fig. 2*B*). To test whether the marked downregulation of p21 was caused by a functional inactivation of p53, P-MEF, I-MEF, I-5, as well as NIH3T3, were treated with nutlin-3. This is a small molecule antagonist of MDM2 that induces p53 and consequently p21 without causing DNA damage (4). Upregulation of p21 both at the transcriptional (Fig. 2*C*) and translational (Fig. 2*D*) levels was found in P-MEF and NIH3T3 with a wild-type p53 but not in I-MEF and I-clones, indicating a nonfunctional p53. In keeping with p53 functional loss all four I-clones are highly aneuploid (hyperdiploid) (1) (Fig. 2*E*); furthermore, they are able to form colonies from single cells (Fig. 2*F*), characteristic of immortal cells.

We have reported that S-MEF showed upregulation of miR-290 and in turn miR-290 overexpression induced premature senescence in P-MEF, suggesting a potential tumor suppressor activity of this miRNA in murine fibroblasts (9).

It was then interesting to verify whether miR-290 were able to induce senescence in immortal clones and if this were p53 dependent or not. To this end we used I-clones, functionally negative for p53, as well as the immortalized NIH3T3 cells, with wild-type p53 (1). First, we quantified the expression of miR-290 and found that in all I-clones as well as in NIH3T3 the expression of this miRNA is markedly downregulated compared with S-MEF and significantly downregulated compared with P-MEF (Fig. 3*A*). Interestingly miR-290 downregulation appears to take place during the immortalization process at the same time as p21 down-

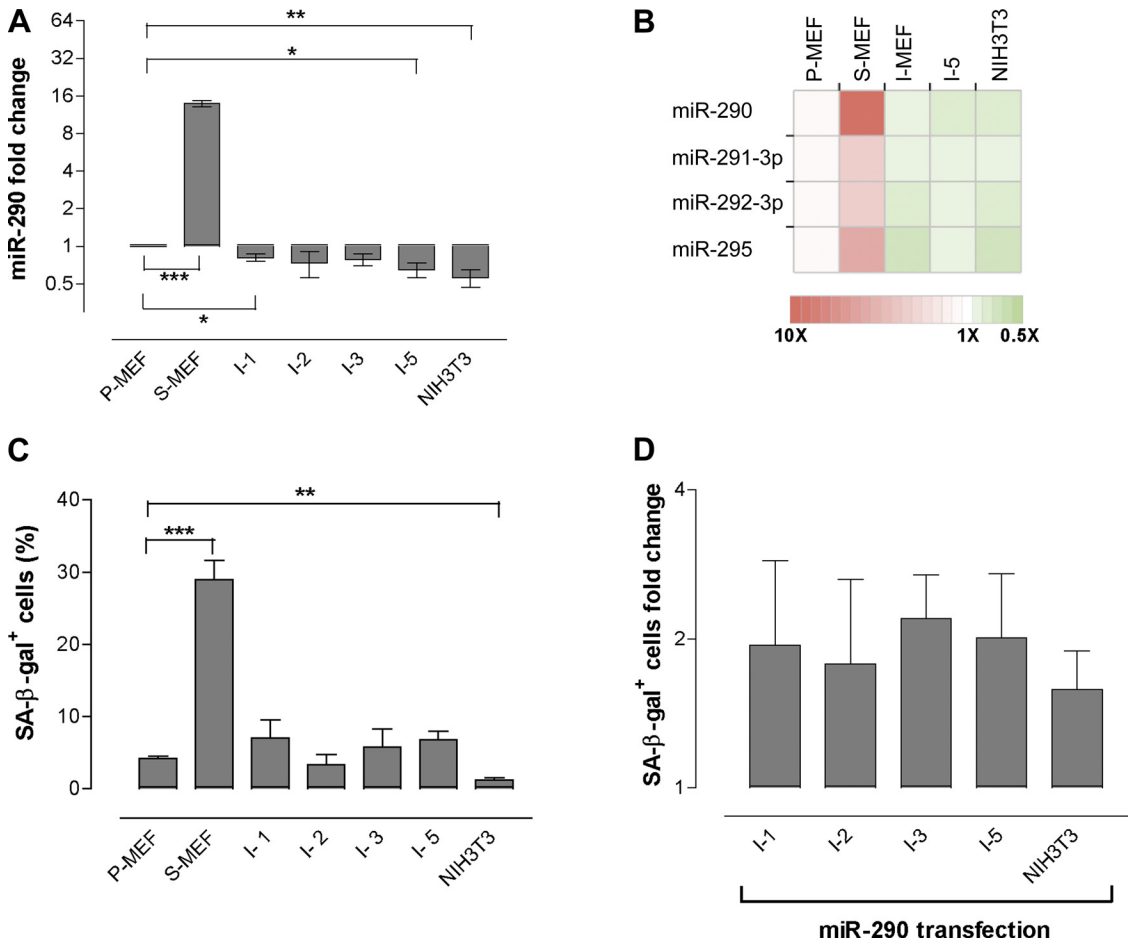

Fig. 3. Responsiveness of I-clones to microRNA (miR)-290 transfection. *A*: expression level of endogenous miR-290 in S-MEF, I-clones (I-1, 2, 3, 5), and NIH3T3 normalized to that of P-MEF; each bar represents the mean ± SD of 3 biological replicates. *B*: heat map reporting the fold change of members of miR-290–295 cluster in S-MEF, I-MEF, I-5, and NIH3T3 normalized to that of P-MEF (1×). *C*: spontaneous level of senescence-associated β-galactosidase (SA-β-gal)$^+$ cells frequency in P-MEF, S-MEF, I-clones, and NIH3T3; the mean ± SD of at least 3 biological replicates are reported. *D*: quantification of SA-β-gal$^+$ cells in I-clones and NIH3T3 cells transfected with miR-290; the mean ± SD of at least 3 biological replicates are reported.

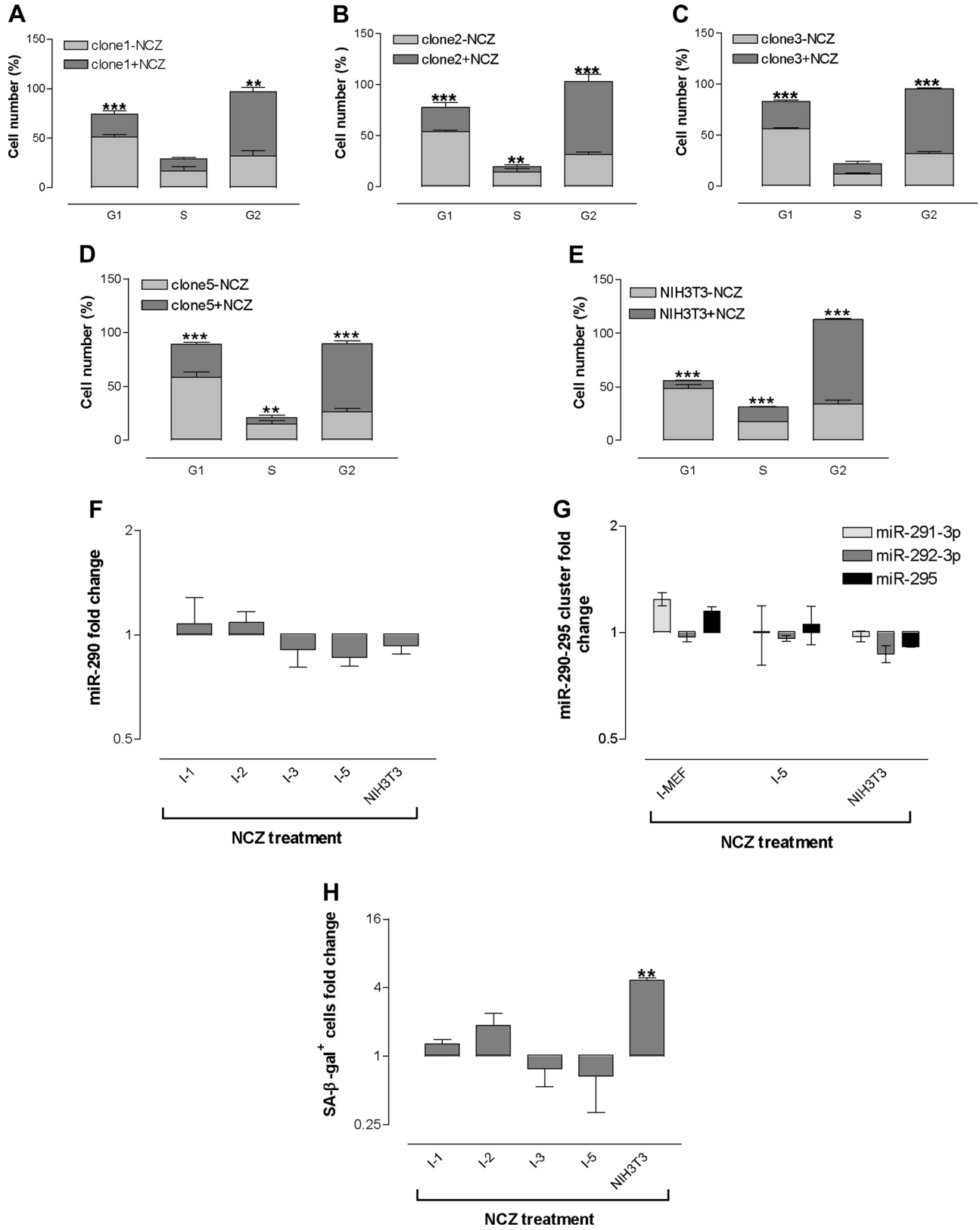

Fig. 4. Responsiveness of I-clones to nocodazole (NCZ). Cell cycle analysis of I-1 (*A*), I-2 (*B*), I-3 (*C*), I-5 (*D*), and NIH3T3 (*E*) cells after 16 h exposure to NCZ; the mean ± SD of at least 3 biological replicates are reported. Quantification of the expression of miR-290 (*F*) and members of miR-290–295 cluster (*G*) and SA-β-gal$^+$ cells induction (*H*) after NCZ treatment; each bar expresses the ratio between miR-290 expression (or SA-β-gal$^+$ cell number) in NCZ-treated cells vs. control cells. The mean ± SD of at least 3 biological replicates are reported.

regulation (11) by an unknown mechanism (genetic or epigenetic silencing, as well as abnormal processing and increased degradation may be responsible). In addition to miR-290, other members of the miR-290–295 cluster (i.e., miR-291–3p, miR-292–3p, and miR-295) were downregulated (Fig. 3*B*), suggesting that either the transcription or the processing of the entire cluster is repressed in immortal MEF. These data also indicate that in I-MEF the miR-290–295 cluster is unlikely to play a prosurvival role similar to that found in mouse embryonic stem cells, where the cluster is overrepresented and prevents apoptosis after genotoxic stress (17). It is worth noting that the low frequency of SA-β-gal$^+$ cells found in I-clones, as well as in NIH3T3 (Fig. 3*C*), correlates with the downregulation of miR-290, in agreement with a potential tumor suppressor role of this miRNA. For these reasons we asked whether overexpression of miR-290 could activate/reactivated the senescence pathway in these immortal clones. The results clearly indicate that miR-290 overexpression, which increased more than fourfold of the percentage of senescent P-MEF (9), neither significantly addresses immortalized cells to senescence (Fig. 3*D*) nor inhibits cell proliferation (data not shown). When the intracellular concentration of miR-290 was measured a significant increase (average 500-fold) was found in all clones, indicating that miR-290 is efficiently transfected into cells. The poor response of NIH3T3 cells to miR-290 suggested that the presence of a functional p53 is not sufficient to reactivate the prosenescence role of miR-290 in immortal cells.

As NCZ, which blocks cells at the G2/M stage, is able to increase P-MEF senescence partially by upregulating miR-290 (9), we asked whether this drug could induce senescence in miR-290-insensitive clones. When either I-clones or NIH3T3 cells were exposed to NCZ, a significant accumulation of cells in G2/M was observed (Fig. 4, *A–E*); however, contrary to what was found in P-MEF (9), miR-290, as well as other members of miR-290–295 cluster, did not change in I-MEF (Fig. 4, *F* and *G*).

These data further support the hypothesis that the cell cycle block imposed by NCZ is miR-290 independent, as previously suggested (9). Interestingly NCZ is able to induce senescence in NIH3T3 (4-fold), while it does not significantly induce senescence in I-clones (Fig. 4*H*). Overall these data indicate that I-clones, lacking a functional p53, are resistant to either miR-290- or NCZ-induced senescence. Conversely NIH3T3 cells with a functional p53, although not responsive to miR-290, are sensitive to NCZ-induced senescence. This result is not unexpected as p53 activity plays a major role in the spindle checkpoint, activated whenever polymerization of spindle microtubules is affected (7). As in NIH3T3 cells, NCZ induces senescence in the absence of miR-290 upregulation, and it is evident that miR-290 is neither a sensor of the cell cycle block nor a physiological effector of senescence in these cells (9). The finding that NCZ does not change significantly the expression of the miR-290–295 cluster in immortal murine fibroblasts with either a nonfunctional (I-MEF and I-clones) or a functional (NIH3T3) p53 is in accordance with the hypothesis that this cluster has a marginal role in these cells.

Overall our data indicate that miR-290 overexpression is not able to address immortalized murine fibroblasts toward senescence, even in the presence of wild-type p53 (NIH3T3); a possible explanation is that the prosenescence targets of miR-290 are missing in these immortal cells. As in P-MEF, miR-290 upregulation always correlated with that of the *INK4a/ARF* locus (9); we hypothesized that a likely (direct or indirect) target of miR-290 could be a repressor of the *INK4a/ARF* locus (9, 12). The high expression of *p19ARF* and *p16* in all immortalized clones, suggestive of repressors loss, is in keeping with this hypothesis. Conversely in NIH3T3 cells where the *INK4a/ARF* locus is deleted (1) miR-290 becomes superfluous.

In conclusion, our data demonstrate that all selected I-MEF clones escape senescence by functionally silencing p53 with consequent downregulation of p21, while the *INK4a/ARF* locus remains expressed. Indeed, contrary to wild-type p53 NIH3T3 cells, I-clones are no longer sensitive to NCZ, a drug that requires a functional p53 to address cells toward senescence. These results are in accordance with the inactivation of the p53 pathway being one of the commonest events in the process of immortalization of murine fibroblasts. An interesting finding of our study is that overexpression of miR-290, markedly downregulated in I-MEF as well as in NIH3T3 cells, is unable to enhance senescence and inhibit cell growth independently of the p53 status. These results suggest that the downregulation of specific miRNAs in tumor cells may be a necessary but not sufficient prerequisite to predict their tumor suppressor activity.

GRANTS

This work was supported by Associazione Italiana per la Ricerca sul Cancro (AIRC project no. 4753) and by Istituto Superiore di Sanità (ISS project no. 527/A/3A/4).

DISCLOSURES

No conflicts of interest, financial or otherwise, are declared by the author(s).

REFERENCES

1. **Calabro V, Parisi T, Di Cristofano A, La Mantia G.** Suppression of Ras-mediated NIH3T3 transformation by p19ARF does not involve alterations of cell growth properties. *Oncogene* 18: 2157–2162, 1999.
2. **Campisi J.** Senescent cells, tumor suppression, and organismal aging: good citizens, bad neighbors. *Cell* 120: 513–522, 2005.
3. **Carnero A, Hudson JD, Hannon GJ, Beach DH.** Loss-of-function genetics in mammalian cells: the p53 tumor suppressor model. *Nucleic Acids Res* 28: 2234–2241, 2000.
4. **Efeyan A, Ortega-Molina A, Velasco-Miguel S, Herranz D, Vassilev LT, Serrano M.** Induction of p53-dependent senescence by the MDM2 antagonist nutlin-3a in mouse cells of fibroblast origin. *Cancer Res* 67: 7350–7357, 2007.
5. **el-Deiry WS, Tokino T, Velculescu VE, Levy DB, Parsons R, Trent JM, Lin D, Mercer WE, Kinzler KW, Vogelstein B.** WAF1, a potential mediator of p53 tumor suppression. *Cell* 75: 817–825, 1993.
6. **Joachimiak MP, Weisman JL, May B.** JColorGrid: software for the visualization of biological measurements. *BMC Bioinformatics* 7: 225, 2006.
7. **Meek DW.** The role of p53 in the response to mitotic spindle damage. *Pathol Biol (Paris)* 48: 246–254, 2000.
8. **Parrinello S, Samper E, Krtolica A, Goldstein J, Melov S, Campisi J.** Oxygen sensitivity severely limits the replicative lifespan of murine fibroblasts. *Nat Cell Biol* 5: 741–747, 2003.
9. **Pitto L, Rizzo M, Simili M, Colligiani D, Evangelista M, Mercatanti A, Mariani L, Cremisi F, Rainaldi G.** miR-290 acts as a physiological effector of senescence in mouse embryo fibroblasts. *Physiol Genomics* 39: 210–218, 2009.
10. **Quelle DE, Zindy F, Ashmun RA, Sherr CJ.** Alternative reading frames of the INK4a tumor suppressor gene encode two unrelated proteins capable of inducing cell cycle arrest. *Cell* 83: 993–1000, 1995.

11. **Rizzo M, Evangelista M, Simili M, Mariani L, Pitto L, Rainaldi G.** Immortalization of MEF is characterized by the deregulation of specific miRNAs with potential tumor suppressor activity. *Aging (Albany NY)* 3: 665–671, 2011.
12. **Rizzo M, Mariani L, Pitto L, Rainaldi G, Simili M.** miR-20a and miR-290, multi-faceted players with a role in tumourigenesis and senescence. *J Cell Mol Med* 14: 2633–2640, 2010.
13. **Ruas M, Peters G.** The p16INK4a/CDKN2A tumor suppressor and its relatives. *Biochim Biophys Acta* 1378: F115–F177, 1998.
14. **Serrano M, Lin AW, McCurrach ME, Beach D, Lowe SW.** Oncogenic ras provokes premature cell senescence associated with accumulation of p53 and p16INK4a. *Cell* 88: 593–602, 1997.
15. **Shen H, Maki CG.** Persistent p21 expression after Nutlin-3a removal is associated with senescence-like arrest in 4N cells. *J Biol Chem* 285: 23105–23114, 2010.
16. **Sherr CJ.** Tumor surveillance via the ARF-p53 pathway. *Genes Dev* 12: 2984–2991, 1998.
17. **Zheng GX, Ravi A, Calabrese JM, Medeiros LA, Kirak O, Dennis LM, Jaenisch R, Burge CB, Sharp PA.** A latent pro-survival function for the miR-290–295 cluster in mouse embryonic stem cells. *PLoS Genet* 7: e1002054, 2011.
18. **Zindy F, Quelle DE, Roussel MF, Sherr CJ.** Expression of the p16INK4a tumor suppressor versus other INK4 family members during mouse development and aging. *Oncogene* 15: 203–211, 1997.